Computational Materials Science 92 (2014) 313–317

Contents lists available at ScienceDirect

Computational Materials Science

journal homepage: www.elsevier.com/locate/commatsci

The relation of mechanical properties and local structures in bulk $Mg_{54}(Cu_{1-x}Ag_x)_{35}Y_{11}$ metallic glasses: *Ab initio* molecular dynamics simulations

Haijun Pan [a], Xiangying Meng [a,*], Qi An [b], Xiaohong Wen [a], Gaowu Qin [a], William A. Goddard III [b]

[a] Key Laboratory for Anisotropy and Texture of Materials (MOE), Northeastern University, Shenyang 110819, China
[b] Materials and Process Simulation Center, California Institute of Technology, Pasadena, CA 91125, USA

ARTICLE INFO

Article history:
Received 26 January 2014
Received in revised form 30 April 2014
Accepted 30 May 2014

Keywords:
Amorphous alloys
Ab initio molecular dynamics
Structure and mechanical properties

ABSTRACT

Understanding the correlation of deformation and local structures in bulk metal glasses (BMGs) is essential for the developing new types of amorphous alloys and their engineering applications. We investigate the relation of local structures and mechanical properties for $Mg_{54}(Cu_{1-x}Ag_x)_{35}Y_{11}$ ($0 < x \leqslant 0.5$) alloys by combining *ab initio* molecular dynamics simulations with density functional theory calculations. It is found that local structures defined by the common-neighbor analysis and mechanical properties display a development as a function of composition, and the calculated results with respect to the Ag composition is well consistent with experiments. We show a strong interplay between local structures and mechanical properties in that high icosahedral ordering and low free volume are helpful to improve the strength, while the incorporation of crystalline ordering and high free volume can initiate a better intrinsic plasticity. Physical implications of these results are discussed and our research is of great value to the development of multi-components amorphous alloys.

1. Introduction

Various studies indicate that mechanical properties of bulk metallic glasses (BMGs) are structural and compositional dependent [1–6]. Unlike crystalline materials, amorphous alloys have random closed-packed structures so that defect based mechanisms (e.g. dislocation, grain boundaries) hardly account for their mechanical properties. The alternative shear transformation zone (STZ) theory [7] suggests that local structure variations in structure are crucial to understand both strength and plastic mechanical behaviors in amorphous alloys. In addition, to pursue high glass forming ability (GFA), the investigations on in multi-composition amorphous alloys is becoming more and more urgent for the design of novel structural materials. However, theoretical researches on bulk metallic glasses were usually limited in binary alloy systems [8–11]. Thus, structural–mechanical relations and rules obtained in binary alloy systems need to be further built and verified in multi-composition amorphous alloy systems, in which makes it interesting to investigate what kind of local structures preferentially undergoes elastic and plastic atomic rearrangement during the evolution stages of deformation process.

Light metal Mg-based alloys in the Mg–Cu–Y systems can be made amorphous over a wide range of compositions leading to BMGs that exhibit both high specific mechanical strength and high elastic limit [12–14]. However, their applications as structural materials are restricted by significant brittleness and low plasticity [15–17]. To address this problem, a modest substitution of Cu by Ag is expected to increase the plasticity of Mg–Cu–Y based amorphous alloys [18]. It is an emerging issue with practical significances to investigate the regulation of mechanical properties by compositional tuning in Mg–Cu–Ag–Y quaternary amorphous alloys.

Using the Mg–Cu–Ag–Y quaternary amorphous alloy as a prototype, we employ *ab initio* molecular dynamics (AIMD) simulations to examine the evolution of local short-range structure when Cu is replaced with Ag in super-cooled $Mg_{54}(Cu_{1-x}Ag_x)_{35}Y_{11}$ ($0 < x \leqslant 0.5$) systems. Furthermore, we use density functional theory (DFT) calculations to determine the structure-related mechanical properties including both elastic moduli and ideal shear strength. We carefully examine the relation of the local structures and mechanical properties with respect to the Ag fraction in $Cu_{1-x}Ag_x$, and extract physical implications. The present studies are scientific benefit to the future design of novel multi-component amorphous alloys.

* Corresponding author. Tel.: +86 2483681159.
E-mail address: x_y_meng@mail.neu.edu.cn (X. Meng).

http://dx.doi.org/10.1016/j.commatsci.2014.05.066
0927-0256/

2. Computational methods

$Mg_{54}(Cu_{1-x}Ag_x)_{35}Y_{11}$ ($0 < x \leqslant 0.5$) amorphous cells were built by filling 200 constituent atoms in a cubic box with periodic boundary conditions, and lengths of the simulation boxes were fixed to reproduce the experimental density at each composition [18]. Our first-principles calculations were carried out using the *ab initio* total energy and molecular dynamics program Vienna *ab initio* simulation package (VASP) [19–21]. For the construction of pseudopotentials (PP) of Mg, Cu, Ag atoms, we treated conventional $3s^2$, $3d^{10}4s^1$, and $4d^{10}5s^1$ as valence electronic configuration throughout this work. For Y rare earth atom, the complete third shell was treated as a core shell, and we arrived at a Y^{11} PP which incorporates $4s^24p^65s^24d^1$ electrons. Perdew–Wang 91 [22] exchange and correlation functional was adopted, and the plane wave cutoff was set to 500 eV. A*b initio* dynamical simulations were performed in the canonical (NVT) ensembles using Nosé thermostats (damping constant 20 fs) to control temperatures. Newton's equations of motion were integrated using the Verlet algorithm with a time step of 2 fs and Γ-point sampling was used to sample Brillouin zone.

To obtain the equilibrium lattices of quenched multi-composition amorphous alloys, each composition alloy was first equilibrated at $T = 2000$ K for 10 ps to eliminate initial unreasonable atom locations, then quenched to a super-cooled temperature lower by ~150 K than experimental glass transition temperatures at a rate of 20 K/ps. We determined the equilibration state from the potential energy evolution and atomic root mean square deviation (RMSD), which remains constant over the duration of the simulation. At the super-cooled temperature, the simulation boxes were equilibrated again for 10 ps. After AIMD procedures, we further relaxed the box parameters and atom positions to release the internal stress using variable cell algorithm within the frame of density functional theory (DFT). In this section, the plane-wave cutoff and *K*-point sampling was changed to 600 eV and $11 \times 11 \times 11$, respectively. The relaxation of geometry was carried out to ensure absolute convergence of the total Hellmann–Feynman force with respect to structural degrees of freedom to the precision of 1 meV/Å, and the final pressures of the amorphous systems were found to be less than 10 MPa.

For each composition, 1000 configurations (snapshots over the last 2 ps) were averaged for the structural analysis. The total pair distribution function (PDF) was calculated with the equilibrated super-cooled BMG boxes, and the total coordination number (CN) was yield by integrating from the first peak up to the first minimum position in PDF.

The inherent structures were analyzed using common neighbor analysis (CNA) proposed by Honeycutt and Anderson [23]. CNA can distinguish between the fcc, hcp, bcc, and icosahedral (ICO) packing in terms of four indices. For instance, 1421 and 1422 bonded pairs are characteristic of close-packed fcc and hcp structures, 1311 bonded pairs represent the rhombus symmetrical features of short range order, and the number of 1551 and 1541 bonded pairs is a direct measure of the degree of ICO ordering.

To analyze the free volume, we discretized space in cells to give each point a value corresponding to the minimum distance separating this point from the closest particle in the network. The covalent radius of the component atoms was chosen as the maximal distance above which a point would be far enough from the closest particles and could therefore be considered in a void zone. To this end, R.I.N.G.S. code [24] was used to facilitate our calculations.

Thermodynamic variable enthalpy is continuous during the liquid-glass transition. However, the derivative of enthalpy (the heat capacity C_p) show an abrupt change at the glass transition temperature T_g, which enables us to predict T_g from the quenching AIMD simulations [25,26]. We extract the enthalpy (H) directly from simulations via the thermodynamic relation $H = PV + U$, where U is the internal energy, P is the pressure, and V is the volume. Also, we can calculate the enthalpy by integrating the specific heat capacity C_p. For solid states the specific heat capacity $C_p = 3R$ (R is the gas constant) following the Dulong–Petit law; while the heat capacity for liquids can be expressed as $C_p = 3R + aT + bT^{-2}$ (T is temperature). By fitting the enthalpy as a function of temperature, the glass transition temperature T_g was determined from the intersection of the solid and liquid enthalpy lines.

Elastic constants were obtained by fitting the second order coefficient in a polynomial of the total energy change ΔE as a function of small fixed distortions δ to the equilibrium lattice. In cubic symmetry, there are three independent elastic constants, *i.e.* C_{11}, C_{12}, and C_{44}. To calculate the C_{11} and C_{12}, we take strains $\xi_1 = (\delta, \delta, 0, 0, 0, 0)$ and $\xi_2 = (\delta, -\delta, \delta^2/(1-\delta^2), 0, 0, 0)$, which results in $\Delta E = V_0(C_{11} + C_{12})\delta^2$ and $\Delta E = V_0(C_{11}-C_{12})\delta^2$, respectively. The energy increment associated with strain $\xi_3 = (0, 0, \delta^2/4, \delta, \delta, 0)$ is $\Delta E = V_0 C_{44}\delta^2$. In the equation, V_0 is the equilibrium volume of the unstrained box.

In the Voigt–Reuss–Hill (VRH) approximation [27], the bulk modulus B, shear modulus G, and Young's modulus E for the cubic box are expressed as $B = (C_{11} + 2C_{12})/3$, $G = (C_{11}-C_{12} + 3C_{44})/5$, and $E = 9BG/(3B + G)$. The Poisson's ratio υ, often used as the indicator for distinguishing tough/ductile BMGs, is determined by $\upsilon = (3B\text{-}E)/6B$.

The ideal shear strength means a failure stress during deforming unconstrained solids, which corresponding to the maximum point in the stress–strain curve. To calculate the ideal shear strength, *x*-vector was selected as perpendicular to the slip plane and *z*-vector parallel to the slip direction in the plane. Incrementally deformed lattices were relaxed with respect to the basis vectors orthogonal to the applied strain and the atoms inside the box. The initial position at each strain step was taken from the relaxed coordinate of previous strain step [28–30].

3. Results and discussion

In Fig. 1, taking $Mg_{54}(Cu_{0.8}Ag_{0.2})_{35}Y_{11}$ as a representative, we illustrate how the structural, thermodynamic, and mechanical parameters are extracted from the AIMD and DFT calculations. Allowing alloy atoms to adjust their positions, RMSD (Fig. 1a) goes down to zero and levels off further on. This is a typical behavior for MD simulations. Leveling of the RMSD means that atoms have relaxed from their initial sits to more stable ones, and the equilibration is assumed to be sufficient when RMSD level disappears. The total PDF curve (Fig. 1b) shows an obvious amorphous structure character, and CN analysis indicate the atoms are average 13.23 coordinate. The variation of enthalpy with respect to the temperature during quenching is illustrated in Fig. 1c. The green solid enthalpy line is fitted from the Dulong–Petit relation in the temperature range of 300–500 K, and the red liquid enthalpy line is fitted from the equation $C_p = 3R + AT + BT^{-2}$ in the temperature range of 600–2000 K. The glass transition temperature T_g is thus determined from the intersection of the fitted solid and liquid enthalpy lines. In Fig. 1d, the deformation energy (ΔE) versus the fixed cell strain δ is plotted on the basis of three types of lattice distortion. We apply a set of given strains with a finite variation between −0.01 and +0.01 within which Hooke's law applies, and the three independent elastic constants C_{11}, C_{12}, and C_{44} are then obtained by means of quadratic fitting. For each composition in $Mg_{54}(Cu_{1-x}Ag_x)_{35}Y_{11}$ ($0 < x \leqslant 0.5$), structural, thermodynamic, and mechanical parameters are listed in Table 1, and compared with available experimental values.

Insight into the structural change as a function of composition can be effectively gained by the common neighbor analysis. Table 1 lists the abundance of main bonded pairs found in super-cooled

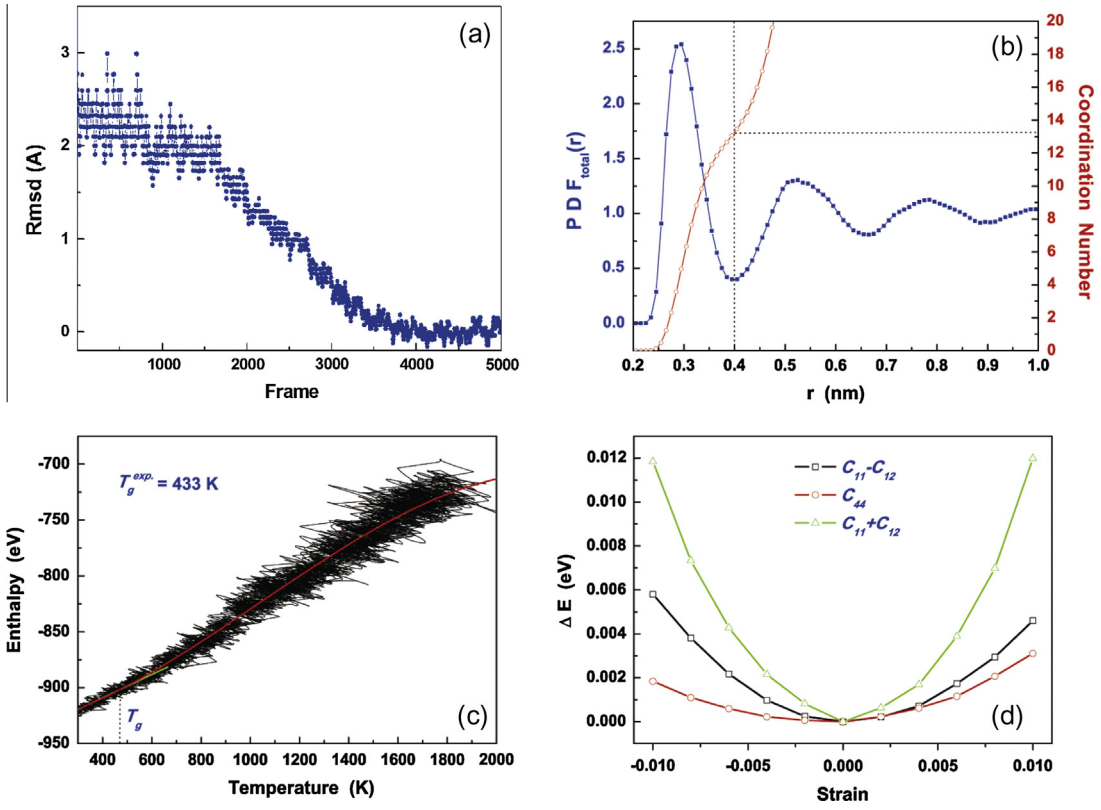

Fig. 1. Illustrations of calculated parameters for $Mg_{54}(Cu_{0.8}Ag_{0.2})_{35}Y_{11}$ system. (a) RMSD trace from AIMD simulations. (b) PDF and CN analysis. (c) The variation of enthalpy in the quenching simulation. (d) Energy–strain curves during the elastic deformation.

Table 1
Structural, thermodynamic, and mechanical parameters in $Mg_{54}(Cu_{1-x}Ag_x)_{35}Y_{11}$ super-cooled amorphous alloys. Various local orders are indicated by four indices. The total coordination number CN, density glass ρ, transition temperature T_g, average bulk modulus $\bar{B}$, shear modulus $\bar{G}$, Young's modulus $\bar{E}$, Poisson ratio $\bar{\nu}$, shear strength σ, and normalized free volume Ω are listed and compared with available experiments.

	x_{Ag} = 0.1	x_{Ag} = 0.2	x_{Ag} = 0.3	x_{Ag} = 0.4	x_{Ag} = 0.5
HC 15xx	856	842	784	762	718
HC 142x	68	80	87	94	98
HC 1311	28	33	36	38	42
CN	13.30	13.23	13.17	13.13	13.07
Lattice (Å)	a = 15.76	a = 15.83	a = 15.83	a = 15.91	a = 15.92
ρ (g/cm^3)	3.962	4.040	4.167	4.235	4.355
	3.96$^{exp.}$	4.03$^{exp.}$	4.17$^{exp.}$	4.23$^{exp.}$	4.35$^{exp.}$
T_g (K)	470	471	473	474	476
	431$^{exp.}$	433$^{exp.}$	435$^{exp.}$	437$^{exp.}$	438$^{exp.}$
$\bar{B}$ (GPa)	53.01	52.22	51.04	49.95	49.41
	52.1$^{exp.}$	52.0$^{exp.}$	53.1$^{exp.}$	52.5$^{exp.}$	52.1$^{exp.}$
$\bar{G}$ (GPa)	26.72	26.13	24.88	24.06	23.02
	20.7$^{exp.}$	20.6$^{exp.}$	20.6$^{exp.}$	20.3$^{exp.}$	20.2$^{exp.}$
$\bar{E}$ (GPa)	69.13	66.04	63.57	62.03	60.79
	54.8$^{exp.}$	54.7$^{exp.}$	54.8$^{exp.}$	54.0$^{exp.}$	53.6$^{exp.}$
$\bar{G}/\bar{B}$	0.504	0.500	0.487	0.483	0.466
	0.40$^{exp.}$	0.40$^{exp.}$	0.39$^{exp.}$	0.39$^{exp.}$	0.39$^{exp.}$
$\bar{\nu}$	0.283	0.289	0.292	0.293	0.295
	0.325$^{exp.}$	0.325$^{exp.}$	0.328$^{exp.}$	0.329$^{exp.}$	0.329$^{exp.}$
Ω	0.040	0.043	0.045	0.047	0.049
σ (GPa)	1.94	1.83	1.70	1.66	1.54

$^{exp.}$ Ref. [18].

amorphous alloys. Frank [31] hypothesized that the local structure of super-cooled melts contains a significant degree of icosahedral short range order (ISRO), which has been observed in previous simulations [32,33]. Recent angstrom-beam electron diffraction experiments also confirm the local icosahedral order in $Zr_{80}Pt_{20}$ metallic glasses [34]. Indeed, Table 1 shows that the 15xx coordination is preponderant over the whole range of compositions verifying that the short range order of $Mg_{54}(Cu_{1-x}Ag_x)_{35}Y_{11}$ BMGs is dominated by the icosahedral and distorted icosahedral short range order. Three kinds of ICO cluster are found in the simulation boxes: two of them are Cu-centered, and the other is Ag-centered. The composition of Cu-centered clusters is $(Mg_8Ag_2Y_1Cu_1)Cu$ and $(Mg_7Ag_1Y_2Cu_2)Cu$, respectively; and that of Ag-centered cluster is $(Mg_8Ag_1Y_1Cu_2)Ag$. To be more intuitive, we provide pictures of observed ICO clusters in Fig. 2.

The contributions of 1311 and 142x pairs related to the rhombus and fcc/hcp local orders are far less important than the 15xx fivefold symmetrical pairs. We notice that with increased Ag fractions, the number of 15xx pairs keep descending, while that of 142x and 1311 pairs continue to rise, suggesting local structural are sensitive to the Ag contents.

In Fig. 2, the statistical average values of the bulk modulus $\bar{B}$, shear modulus $\bar{G}$, and Young's modulus $\bar{E}$ in view of selected five snapshots with error bar estimation are plotted. By comparing elastic moduli with the number of atomic ordering of each composition, we observe a clear correlation between ISRO and elastic moduli: ISRO, $\bar{B}$, $\bar{G}$, and $\bar{E}$ present the same trend, and derived $\bar{G}/\bar{B}$ and Poisson's ratio $\bar{\nu}$ also display a strong dependence on the ISRO pair. This validates that ISRO is the key structural feature in the $Mg_{54}(Cu_{1-x}Ag_x)_{35}Y_{11}$ $(0 < x \leqslant 0.5)$ BMGs that controls elastic parameters, namely B, G, E, G/B and ν. The calculated tendency of elastic moduli with respect to the Ag composition is well consistent with previous experiments [18], in which however the inner relevance between mechanical properties and ISRO has not been established due to the experimental failure to detect atomic orderings.

The BMGs having lower G/B and higher ν are believed to exhibit better intrinsic plasticity [35,7,36]. Based on our structure-elastic

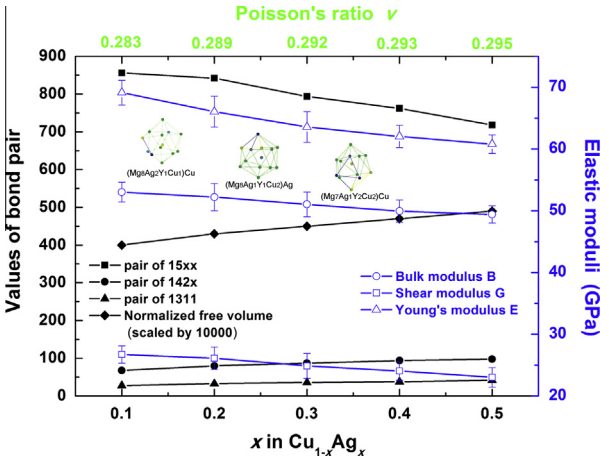

Fig. 2. Local orders, normalized free volume and elastic parameters with respect to the Ag fractions in $Mg_{54}(Cu_{1-x}Ag_x)_{35}Y_{11}$ super-cooled BMGs. The observed icosahedral clusters in the simulation boxes are also presented.

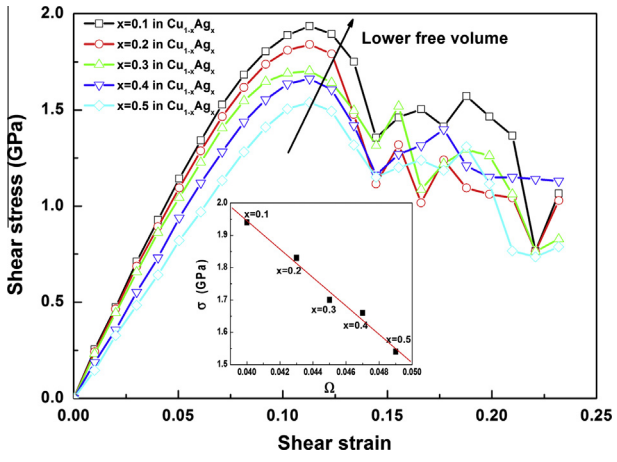

Fig. 4. Shear stress–strain curves of $Mg_{54}(Cu_{1-x}Ag_x)_{35}Y_{11}$ super-cooled BMGs. In the sub-plotting, the relationship between the ideal shear strength and the normalized free volume is presented for different Ag fractions.

modulus relations, we find that the plasticity of BMGs decreases with the icosahedral ordering, but increases with the rhombus and fcc/hcp local ordering. Thus we expect that the incorporation of crystalline ordering into amorphous alloys can enhance the plastic performance of BMGs.

To found the electronic origin of elastic moduli, we studied electronic partial density of states (PDOS) for different composition alloys. In Fig. 3, the isolated PDOS peaks contributed by Y 5*s* and 4*p* are found to be located at deep energy levels. The weak *s*-hybridizations between Mg 3*s*, Cu 4*s*, and Ag 5*s* take place around the Fermi level, which has been set as a reference level. With the increased Ag fractions, we notice that the hybridization between Cu 3*d* and Ag 4*d* is increasing while between Cu 3*d* and Y4*d* is decreasing, giving it a stronger Cu–Ag but weaker Cu–Y bonding nature. In our latest work [37], we revealed that the bulk modulus and strength of alloys are affected by the degree of localization of valence electrons. Thus the electronic origin of the high elastic moduli may be attributed to the interaction between unsaturated Y 4*d* and Cu 3*d* electrons; while Cu 3*d* and Ag 4*d* are all saturated and their bonds will result a lower elastic moduli.

To explore the strength mechanism, we further investigate the relation between the shear strength and the free volume that has been normalized by the total volume of $Mg_{54}(Cu_{1-x}Ag_x)_{35}Y_{11}$ ($0 < x \leqslant 0.5$) super-cooled amorphous cells. In Fig. 4, it is clear that the maximum value of the ideal stress–strain curve, namely the ideal shear strength, increases with the decreasing free volume in $Mg_{54}(Cu_{1-x}Ag_x)_{35}Y_{11}$ BMGs. The calculated relationship between the ideal shear strength σ and the normalized free volume Ω are presented in the sub-plot of Fig. 4, suggesting a logarithmic relationship between σ and Ω with the form of $log(\sigma) = a + b \times \Omega$ [38,39].

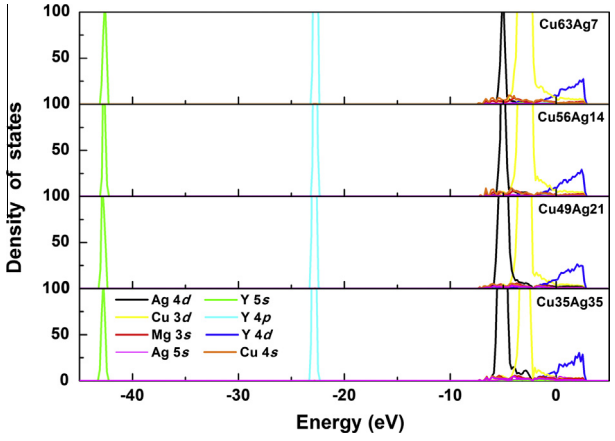

Fig. 3. The electronic partial density of states (PDOS) of $Mg_{54}(Cu_{1-x}Ag_x)_{35}Y_{11}$ super-cooled BMGs. In the plotting, the Fermi level has been set as a reference energy level.

In BMGs, the plastic deformation occurs in shear and the ideal shear strength indicates the resistance of a material against plastic deformation. Since plastic deformations involve states far from the equilibrium, with the decreased Ag content, BMGs having lower free volume require more stress to shift atoms away from their sites, resulting in a higher shear strength. On the other hand, the incorporation of Ag allows a higher free volume and provides a larger void zone to offset atoms destructive deformation, thus exhibits a better plasticity. The structural parameters in Table 1 shows that with the increased Ag content, lower 15xx CN results in a lower CN number but a higher free volume. Thus, high ISRO can not only induce larger elastic moduli, such as *B*, *G*, and *E*, but also guarantees a stronger shear strength in $Mg_{54}(Cu_{1-x}Ag_x)_{35}Y_{11}$ BMGs.

4. Conclusion

In summary, combining AIMD simulations with DFT calculations, we investigated structure-mechanics relations in $Mg_{54}(Cu_{1-x}Ag_x)_{35}$-$Y_{11}$ BMGs. These relations provide new insights about the elastic modulus, strength and plasticity in multi-composition BMGs, from the perspective of local structures. We find that elastic moduli are basically determined by the number of icosahedral orderings. High ISRO and low free volume are helpful to improve elastic moduli and the strength of BMGs, while the incorporation of crystalline ordering and high free volume can initiate a better intrinsic plasticity in BMGs. We need a balance between the strength and plastic properties according to the practical requirements, and such a choice can thus be achieved based on the theoretical virtual component regulation and structural analysis during the development of multi-composition amorphous alloys.

Acknowledgments

This work is financial supported by the Fundamental Research Funds for the Central Universities (N130405003), National Natural Science Foundation of China (No. 51001025), and National High

Technology Research and Development Program of China (Grant No. 2013AA031601). Q.A. and W.A.G. thank NSF DMR-0520565 Caltech CSEM for support.

References

[1] E.S. Park, D.H. Kim, Met. Mater. Inter. 11 (2005) 19.
[2] J. Schroers, W.L. Johnson, Phys. Rev. Lett. 93 (2004) 255506.
[3] M.W. Chen, NPG Asia Mater. 3 (2011) 82.
[4] Y.Q. Cheng, A.J. Cao, E. Ma, Acta Mater. 57 (2009) 3253.
[5] W.H. Wang, C. Dong, C.H. Shek, Mater. Sci. Eng. R 44 (2004) 45.
[6] Q. He, Y.Q. Cheng, E. Ma, J. Xu, Acta Mater. 59 (2011) 202.
[7] A.S. Argon, Acta Metall. 27 (1979) 47.
[8] C.G. Tang, P. Harrowell, Nat. Mater. 12 (2013) 507.
[9] M. Imran, F. Hussain, M. Rashid, Y.Q. Cai, S.A. Ahmad, Chin. Phys. B 22 (2013) 096101.
[10] M. Durandurdu, Comp. Mater. Sci. 65 (2012) 44.
[11] N.P. Bailey, J. Schiøtz, K.W. Jacobsen, Mater. Sci. Eng. A 387–389 (2004) 996.
[12] A. Inoue, K. Ohtera, K. Kita, T. Masumoto, Jpn. J. Appl. Phys. 27 (1998) L2248.
[13] A. Inoue, M. Kohinata, A.P. Tsai, T. Masumoto, Mater. Trans. JIM 30 (1989) 378.
[14] A. Inoue, K. Ohtera, M. Kohinata, A.P. Tsai, T. Masumoto, J. Non-Cryst. Solids 712 (1990) 117.
[15] C.A. Schuh, T.C. Hufnagel, U. Ramamurty, Acta Mater. 55 (2007) 4067.
[16] M. Ashby, A.L. Greer, Scr. Mater. 54 (2006) 321.
[17] J. Xu, U. Ramamurty, E. Ma, JOM 62 (2010) 10.
[18] S.G. Wang, L.L. Shi, J. Xu, J. Mater. Res. 26 (2011) 923.
[19] G. Kresse, J. Hafner, Phys. Rev. B 48 (1993) 13115.
[20] G. Kresse, J. Furthmuller, Phys. Rev. B 54 (1996) 11169.
[21] G. Kresse, J. Furthmuller, Comp. Mater. Sci. 6 (1996) 15.
[22] Y. Wang, J.P. Perdew, Phys. Rev. B 44 (1991) 13298.
[23] J.D. Honeycutt, H.C. Andersen, J. Phys. Chem. 91 (1987) 4950.
[24] S.L. Roux, P. Jund, Comp. Mat. Sci. 49 (2010) 70.
[25] R. Busch, Y.J. Kim, W.L. Johnson, J. Appl. Phys. 77 (1995) 4039.
[26] Q. An, K. Samwer, W.A. Goddard III, W.L. Johnson, A.J. Botero, G. Garret, M.D. Demetriou, J. Phys. Chem. Lett. 3 (2012) 3143.
[27] D. Chung, Philos. Mag. 8 (1963) 833.
[28] R.F. Zhang, S. Veprek, Phys. Rev. B 77 (2008) 172103.
[29] D. Roundy, C.R. Krenn, M.L. Cohen, J.W. Morris Jr., Phys. Rev. Lett. 82 (1999) 2713.
[30] R.F. Zhang, S.H. Sheang, S. Veprek, Appl. Phys. Lett. 90 (2007) 191903.
[31] F.C. Frank, Proc. R. Soc. London, Ser. A 215 (1950) 1022.
[32] Y. Qi, T. Cagin, W.L. Johnson, W.A. Goddard III, J. Chem. Phys. 115 (2001) 385.
[33] H.J. Lee, T. Cagin, W.L. Johnson, W.A. Goddard III, J. Chem. Phys. 119 (2003) 9858.
[34] A. Hirata, L.J. Kang, T. Fujita, B. Klumov, K. Matsue, M. Kotani, A.R. Yavari, M.W. Chen, Science 341 (2013) 376.
[35] L. Zhang, Y.Q. Cheng, A.J. Cao, J. Xu, E. Ma, Acta Mater. 57 (2009) 1154.
[36] D.W. He, S.R. Shieh, T.S. Duffy, Phys. Rev. B 70 (2004) 184121.
[37] D.Y. Liu, H.J. Pan, X.Y. Meng, Model. Simul. Mater. Sci. Eng. 22 (2014) 055017.
[38] P.K. Watson, J.M. Valverde, A. Castellanos, Powder Technol. 115 (2001) 45.
[39] N. Jakse, A. Pasturel, Phys. Rev. B 78 (2008) 214204.